Atmos. Meas. Tech. Discuss., 8, 4273–4305, 2015
www.atmos-meas-tech-discuss.net/8/4273/2015/
doi:10.5194/amtd-8-4273-2015

Atmospheric Measurement Techniques Discussions
Open Access

Optimization of the GSFC TROPOZ DIAL retrieval using synthetic lidar returns and ozonesondes – Part 1: Algorithm validation

J. T. Sullivan[1,2], T. J. McGee[3], T. Leblanc[4], G. K. Sumnicht[5], and L. W. Twigg[5]

[1]Department of Atmospheric Physics, University of Maryland, Baltimore County (UMBC), Baltimore, MD, USA
[2]Joint Center for Earth Systems Technology (JCET), Baltimore, MD, USA
[3]Atmospheric Chemistry and Dynamics Laboratory, NASA Goddard Space Flight Center, Greenbelt, MD, USA
[4]California Institute of Technology, Jet Propulsion Laboratory, Wrightwood, CA, USA
[5]Science Systems and Applications Inc., Lanham, MD, USA

Received: 11 February 2015 – Accepted: 10 April 2015 – Published: 28 April 2015

Correspondence to: J. T. Sullivan (johnsullivan@umbc.edu)

Published by Copernicus Publications on behalf of the European Geosciences Union.

Abstract

The main purpose of the NASA Goddard Space Flight Center TROPospheric OZone DIfferential Absorption Lidar (GSFC TROPOZ DIAL) is to measure the vertical distribution of tropospheric ozone for science investigations. Because of the important health and climate impacts of tropospheric ozone, it is imperative to quantify background photochemical and aloft ozone concentrations, especially during air quality episodes. To better characterize tropospheric ozone, the Tropospheric Ozone Lidar Network (TOLNet) has recently been developed, which currently consists of five different ozone DIAL instruments, including the TROPOZ. This paper addresses the necessary procedures to validate the TROPOZ retrieval algorithm and develops a primary standard for retrieval consistency and optimization within TOLNet. This paper is focused on ensuring the TROPOZ and future TOLNet algorithms are properly quantifying ozone concentrations and the following paper will focus on defining a systematic uncertainty analysis standard for all TOLNet instruments.

Although this paper is used to optimize the TROPOZ retrieval, the methodology presented may be extended and applied to most other DIAL instruments, even if the atmospheric product of interest is not tropospheric ozone (e.g. temperature or water vapor). The analysis begins by computing synthetic lidar returns from actual TROPOZ lidar return signals in combination with a known ozone profile. From these synthetic signals, it is possible to explicitly determine retrieval algorithm biases from the known profile, thereby identifying any areas that may need refinement for a new operational version of the TROPOZ retrieval algorithm. A new vertical resolution scheme is presented, which was upgraded from a constant vertical resolution to a variable vertical resolution, in order to yield a statistical uncertainty of $< 10\,\%$. The optimized vertical resolution scheme retains the ability to resolve fluctuations in the known ozone profile and now allows near field signals to be more appropriately smoothed. With these revisions, the optimized TROPOZ retrieval algorithm ($\mathrm{TROPOZ_{opt}}$) has been effective in retrieving nearly 200 m lower to the surface. Also, as compared to the previous version

AMTD
8, 4273–4305, 2015

of the retrieval, the TROPOZ$_{opt}$ has reduced the mean profile bias by 3.5 % and large reductions in bias (near 15 %) were apparent above 4.5 km.

Finally, to ensure the TROPOZ$_{opt}$ retrieval algorithm is robust enough to handle actual lidar return signals, a comparison is shown between four nearby ozonesonde measurements. The ozonesondes agree well with the retrieval and are mostly within the TROPOZ$_{opt}$ retrieval uncertainty bars (which implies that this exercise was quite successful). A final mean percent difference plot is shown between the TROPOZ$_{opt}$ and ozonesondes, which indicates that the new operational retrieval is mostly within 10 % of the ozonesonde measurement and no systematic biases are present. The authors believe that this analysis has significantly added to the confidence in the TROPOZ instrument and provides a standard for current and future TOLNet algorithms.

1 Introduction

Ozone above the ground level has been historically difficult to measure directly due to its relatively short lifetime and nonlinear formation (Stevenson et al., 2013). It is an important greenhouse gas, pollutant, and source of OH radicals. Its contribution to global warming from the preindustrial era to the present is regarded as the third most important, following those of carbon dioxide (CO_2) and methane (CH_4) (IPCC, 2007). Ozone is also toxic to humans and vegetation because it can oxidize biological tissue and may cause harmful respiratory effects in instances of long exposure (McDonnell et al., 1999). Ozone may also be transported aloft or advected with varying layer thickness and concentration downwind of the major ozone precursor production sites, potentially resulting in an ozone exceedance for rural and less populated areas (NCA, 2013; Langford et al., 2010). Because of these important climate and health impacts and the possibility of layers of ozone aloft, it is important to produce validated and quantitative ozone concentration profiles.

The ground based Goddard Space Flight Center TROPospheric OZone DIfferential Absorption Lidar (GSFC TROPOZ DIAL) has been routinely taking measurements in

AMTD
8, 4273–4305, 2015

the Baltimore-Washington D.C. region (Greenbelt, MD 38.99° N, 76.84° W, 57 m a.s.l.) from a 13 m transportable trailer since Fall of 2013. Many of the instrument and current retrieval specifications can be found in Sullivan et al. (2014). This instrument has been developed as part of the ground-based Tropospheric Ozone Lidar NETwork (TOLNet), which currently consists of five stations across the United States (http://www-air.larc.nasa.gov/missions/TOLNet/). Because this network consists of five different ozone lidar systems, it is important that retrievals for each site be independently validated and cross-compared to provide accurate information for future science campaigns. For this reason, this paper addresses the necessary procedures to validate the TROPOZ retrieval algorithm as well as develops a primary standard for the consistency and optimization of ozone retrievals within TOLNet.

Aside from the algorithm optimization analysis presented in this work, several retrieval intercomparisons have also been performed to help aid in network consistency. In May 2014, an intercomparison between the TROPOZ and the Langley Mobile Ozone Lidar (LMOL, Pliutau and De Young, 2013), was performed in which no biases were apparent as compared to ozonesonde profiles when retrievals were performed with adequate signal (Sullivan et al., 2014, 2015). Additionally, the TROPOZ and NOAA TOPAZ (Tunable Optical Profiler for Aerosol and oZone lidar, Alvarez et al., 2011) were operated simultaneously for several days in July 2014 and a detailed intercomparison analysis is currently being performed.

The most common method for validation of ozone lidars is a comparison with a balloon-borne electrochemical concentration cell (ECC) ozonesonde (Ancellet et al., 1989; McDermid et al., 2002; Kuang et al., 2013; Uchino et al., 2014). The ECC profiles ozone from the surface to a balloon dependent altitude (Komhyr et al., 1995; Thompson et al., 2003; Newchurch et al., 2003). Many research groups have long term records of ozone soundings using this method, but small correction factors may be necessary depending on the manufacturer or the cathode solution used. For measurement of ozone below 30 km with these correction factors, ECC ozonesondes yield a precision better than ±3 – 5 % and an accuracy of about ±5 – 10 % (Smit et al., 2007).

AMTD
8, 4273–4305, 2015

Although ozonesondes may be a useful validation tool, the instantaneous measurement may not be able to fully characterize small scale fluctuations in ozone (Beekmann et al., 1994). The balloon may also be transported a non-negligible distance away from the ozone lidar, resulting in a large difference in resolved air mass. For these reasons, this paper describes the usefulness of utilizing synthetic lidar return signals and a known ozone profile as an independent validation method in addition to nearby ozonesonde launches. Using simulated lidar data instead of an ozonesonde profile is advantageous because by varying parameters in the modeled return signal, it is possible to explicitly determine both the source and the magnitude of various biases in the retrieval from the original ozone profile (Keckhut et al., 2004a).

Similar synthetic signal analyses have been previously performed which focus on the stratosphere (Leblanc et al., 1998); however, this work investigates the processes relevant to tropospheric ozone that are critical for studying air quality impacts. This is also a key region of the atmosphere in which satellites lose the ability to distinguish fine scale ozone features. Future efforts to validate satellite retrieval of tropospheric ozone will require support from reliable ozone profiles from validated and optimized instruments, such as those within TOLNet.

This paper addresses the necessary procedures to validate the optimized TROPOZ retrieval algorithm ($\text{TROPOZ}_{\text{opt}}$) and confirm that it is properly representing ozone concentrations. This process also prevents errors in the retrieval process from invalidating quality data. The following paper in this series will follow a similar methodology and focus on a systematic uncertainty analysis. The parameters investigated within this paper are the corrections that occur naturally from spectral properties of trace gases within the atmosphere (including ozone) and limitations of the hardware used to acquire the data. The numerical derivative is analyzed first to show that it is being performed correctly. Because of naturally varying temperatures in the atmosphere, the temperature dependence of the ozone absorption cross sections is analyzed. The DIAL measurement involves two wavelengths and a correction for the differential spectral-based scattering properties of the Rayleigh atmosphere is investigated. In a photon-counting data

AMTD
8, 4273–4305, 2015

acquisition system, a pulse pile-up correction is often required and is explicitly analyzed in this paper. Vertical resolution is also investigated as it can be a controlling factor in representing the correct ozone profile, especially in the upper free troposphere with a decreasing signal to noise ratio (SNR). All of these corrections and refinements were implemented into the new TROPOZ$_{opt}$ retrieval algorithm and the final section of this paper shows a comparison with good agreement (< 10 %) with four nearby ozonesonde profiles.

2 The DIAL equation

Lidar return signals are not recorded or analyzed as continuous functions, but rather as values in discrete range bins, r. It is possible to write the DIAL equation (Megie et al., 1985) in terms of the range bins specified as

$$N_{O_3}(r) = \frac{1}{2\Delta\sigma_{O_3}} \frac{d}{dr}\left[\ln\left(\frac{P_{on}(r)}{P_{off}(r)}\right) - \ln C\right] - D, \quad (1)$$

where,

$$C = \frac{\beta_{on}(r)}{\beta_{off}(r)} \quad (2)$$

and with aerosols and additional interfering gases,

$$D = \frac{\Delta\alpha_{mol}}{\Delta\sigma_{O_3}} + \frac{\Delta\alpha_{aer}}{\Delta\sigma_{O_3}} + \frac{N_{IG}\Delta\alpha_{IG}}{\Delta\sigma_{O_3}}. \quad (3)$$

For these equations, N_{O_3} is the ozone number density and $\Delta\sigma_{O_3}$ ($\Delta\sigma_{on} - \Delta\sigma_{off}$) is the difference in corresponding ozone absorption cross sections taken at the two DIAL wavelengths. The optical power returned to the receiver, atmospheric backscatter coefficient, and atmospheric extinction coefficient at range r at either the "on" or "off"

AMTD
8, 4273–4305, 2015

wavelength are denoted as P, β and α respectively. The $\Delta\alpha$ ($\Delta\alpha_{on} - \Delta\alpha_{off}$) in Eq. (3) is comprised of the differences between the two DIAL wavelengths in the extinction coefficient for Rayleigh, aerosol, and other interfering gases in the atmosphere.

As evidenced by Eq. (1), DIAL is a self calibrating technique that permits the retrieval of ozone number density from only the known ozone absorption cross sections, the optical power returned to the receiver at each wavelength, and some basic atmospheric backscatter and extinction properties. The power returned back to the detector is the sum of laser light backscattered from molecules and particulates in the atmosphere and ambient background sky radiation. Therefore, P_{off} and P_{on} are actually comprised of $P_{off} + P_b$ and $P_{on} + P_b$, where P_b is the background radiation at the respective wavelengths.

The correction term Eq. (2) is due to the spectral difference in the amount of photons that have undergone Rayleigh backscatter into the detectors from the ambient atmosphere. The first term in Eq. (3) expresses the correction due to the wavelength dependence of Rayleigh extinction, and is easily determined with additional meteorological information given by a reference standard atmosphere (US Standard, 1976). With the knowledge of the Rayleigh extinction values, the Rayleigh backscatter term in Eq. (2) is computed using the assumed Rayleigh phase function. The implementation of this correction is discussed in a later section of this paper.

It is known that a large aerosol loading may cause a significant error in the ozone retrieval, but this can be difficult to correct for without aerosol vertical information (Browell et al., 1985). Because the aerosol profile will never be exactly known, simulating a truth aerosol profile (either from a climatology or previous observations) would yield little information about the retrieval's ability to correct for aerosols during actual observations. For these reasons, aerosols and interfering gases are not analyzed explicitly in this analysis. However, the impacts of aerosols and interfering gases (mainly anomalously large concentrations of SO_2 and NO_2) may be substantial in the overall retrieval uncertainty and will be discussed in a following paper that will focus on the uncertainty in the TROPOZ measurement.

AMTD
8, 4273–4305, 2015

3 Synthetic lidar returns and initial retrieval

In order to validate the GSFC TROPOZ DIAL retrieval algorithm, synthetic lidar return signals have been generated using physical parameters of the lidar system, climatological data, and a known ozone profile. The purpose of generating these synthetic signals is to investigate various parts of the retrieval algorithm with the ability to turn varying effects, such as ambient background radiation, saturation effects, or spectral properties of the atmosphere, on or off. With the ability to vary these effects and decompose the synthetic signals, the TROPOZ retrieval algorithm can be tested in a rigorous manner in order to identify any uncertainty and bias with the original ozone profile.

The synthetic data is based upon various physical components of the lidar system, such as the Field of View (FOV) of each of the detectors, filter bandwidths, the altitudes at which the signals were gated, and the assumption that the signal can be corrected using a nonparalyzable dead time correction for the photomultiplier tubes (PMTs). The saturation correction is based on the laser repetition rate and the photon counting rate of the data acquisition system. The synthetic signals were also modeled from the standard meteorological atmosphere from the TROPOZ site elevation, latitude, and longitude. In order to properly represent the magnitudes of the synthetic signal, cloud free, nighttime data was used to simulate realistic lidar return signal levels. These signals were made from 10 min averages of acquired data, which is a typical temporal resolution for the TROPOZ retrieved ozone concentrations.

The synthetic signals were computed using a known atmospheric state produced by the empirical model MSISE-90 (Hedin, 1991) between the ground and the thermosphere. The model computes a temperature profile and profiles of the main atmospheric constituents' number densities including N_2, O_2, and Ar for a given day-of-year and time-of-day. Though the profiles are not as close to actual profiles as they could be if measured from datasets such as radiosoundings, the model has the advantage of producing smooth, uninterrupted profiles throughout the entire lidar altitude range without having to cope with issues associated with the merging of multiple datasets. In

AMTD
8, 4273–4305, 2015

addition to temperature (T), N_2, O_2, and Ar, the atmospheric state includes an ozone number density profile computed from a combination of climatologies taken from the UK Universities Global Atmospheric Modelling Programme (UGAMP) Thuburn (1992) and from the UARS Reference Atmosphere Project.

After the TROPOZ retrieval was performed on the synthetic return signals, a final ozone concentration profile was computed. It was then possible to truly compare the final ozone profile to the truth profile originally used to produce the simulated synthetic signals. This is not entirely possible with co-located launches of ozonesondes and this emphasizes the advantage of using simulated data as an independent validation source.

Figure 1 shows the initial TROPOZ retrieved ozone mixing ratio (MR) and its associated ozone differences from the modeled truth profile (red) from 0.675 to 10 km. This is a composite profile which represents two different signal pairs from 0.675 to 2.75 km and from 2.75 to 10 km. The definition of the relative percent difference used for Fig. 1, as well as throughout this paper, is

$$\Delta N_{O_3}(\%) = \frac{\text{TROPOZ}_{N_{O_3}} - \text{Model}_{N_{O_3}}}{\text{Model}_{N_{O_3}}} \times 100. \quad (4)$$

This retrieval has been performed with a constant 375 m vertical resolution below 2.75 km and a 750 m vertical resolution above 2.75 km. For the region above 4.5 km, this fixed vertical resolution starts to yield large ozone differences near 15 %, which can certainly be improved upon and are most likely directly attributed to smoothing effects. Also, near the bottom of the profile and near the join region (2.75–3 km), there is a comparably large ozone difference, which will be discussed in a later section of this work. Although the differences between the initial and final ozone profiles in Fig. 1 are mostly within 15 %, there are still underlying biases that may be reduced and this is the motivation for the following sections of this paper.

AMTD
8, 4273–4305, 2015

3.1 Numerical derivative

The first step in ensuring that the DIAL retrieval algorithm is accurate is to confirm that the derivative of the natural logarithm of the ratio of backscattered laser signals from Eq. (1) is correctly calculated. For this reason, synthetic lidar returns were simulated to ensure the proper computation of the numerical derivative. The statistical and background noise, saturation correction, and Rayleigh correction were all removed for this simulation and constant ozone absorption cross sections were used with values of $\sigma_{O_3 299} = 4.200e^{-23}\,m^2$ and $\sigma_{O_3 289} = 1.542e^{-22}\,m^2$ (Malicet et al., 1995).

The finite impulse response (FIR) Savitzky Golay (SG) differentiation filter (Savitzky and Golay, 1964) is used for the numerical derivative and acts as a smoothing filter by neglecting large noise spikes. The SG filter is a generalized running average with coefficients determined by an unweighted linear least-squares regression and a 2nd degree polynomial model applied to the derivative. The second degree is chosen, instead of a third or fourth, because it is less likely to pick up extreme noise. The other advantage of using the SG is that the final vertical resolution of the retrieved ozone can be easily determined using the full width at half maximum (FWHM) of the steady state SG filter coefficients associated with the smoothing window size. To emphasize the possible biases from the numerical derivative, the retrieval is done with a minimal 3 point smoothing.

The results for using the SG filter are shown in Fig. 2, where the left panel shows the final retrieved ozone mixing ratio from the TROPOZ numerical derivative (blue) as compared to the known ozone profile (red) used in the simulated lidar return signal. Both profiles are in the figure but are directly overtop of each other, indicating the numerical derivative is being properly computed in the retrieval algorithm. The right panel shows the negligible percent difference between the known profile and retrieved profile and this will continue to be used as the method of numerical differentiation in the new operational version of the $\text{TROPOZ}_{\text{opt}}$ ozone retrieval.

AMTD
8, 4273–4305, 2015

3.2 Temperature dependence of the ozone absorption cross section

Due to a known temperature dependence of the ozone absorption cross sections (Malicet et al., 1995), it was necessary to get an accurate atmospheric temperature profile, either from a co-located radiosonde launch or from a standard model atmosphere. Because the ozone absorption temperature dependence is not known continuously, but rather at discrete temperatures, and therefore various interpolations have been investigated. These interpolations will affect the $\Delta\sigma_{O_3}$ term in the denominator from Eq. (1) for the final $TROPOZ_{opt}$ retrieval.

In the left panel of Fig. 3, ozone mixing ratios are retrieved using the constant ozone absorption cross sections of $\sigma_{O_3 299} = 4.200e^{-23}\,m^2$ and $\sigma_{O_3 289} = 1.542e^{-22}\,m^2$ and with varying temperature interpolations (Malicet et al., 1995). The statistical and background noise, saturation correction and Rayleigh correction were all removed for this simulation. One profile corresponds to a constant value of $\Delta\sigma_{O_3}$ and additional profiles use a different interpolation of the ozone absorption cross sections. Although the final ozone mixing ratios look very similar to the truth profile for each temperature interpolation, the right panel of Fig. 3 shows subtle differences between the various interpolation schemes (De Boor et al., 1978). For Spline fitting, the interpolated value at a query point is based on a cubic interpolation of the values using not-a-knot conditions at neighboring grid points. For Linear and Cubic fitting, the interpolated value at a query point is based on linear and cubic interpolation of the values. For Nearest fitting, the interpolated value at a query point is the value at the nearest sample grid point.

Regardless of the interpolation used for the synthetic return, the final ozone differences are all mostly within 2 % of the known ozone profile. The blue line, representing a constant temperature value, emphasizes the importance of correcting the TROPOZ retrieval algorithm for temperature, especially in the first few kilometers of the troposphere. The lower portion of this region, known as the Planetary Boundary Layer (PBL), has many stratified temperature layers and inversions, in which an accurate ozone mix-

AMTD
8, 4273–4305, 2015

ing ratio requires an interpolated scheme. Based on the right panel in Fig. 3, most of these interpolations yield a similar bias (within ±1 %) at altitudes above 4.5 km.

Although these percent differences are based on the difference between the cross sections used in the synthetic simulation and the retrieval algorithm, it is important to quantify the magnitude of the bias associated with using a constant cross section and with each of the various interpolations. Based on the biases shown from these interpolations, the TROPOZ$_{opt}$ retrieval algorithm will implement the Cubic interpolation of the temperature dependence of the ozone absorption cross sections.

3.3 Rayleigh molecular extinction

Up until this point, the DIAL Eq. (1) without the corrections from Eqs. (2) and (3) has been satisfactorily investigated. The Rayleigh molecular backscatter (Eq. 2) and extinction (Eq. 3) corrections, which are based on spectral properties of the atmosphere, have now been implemented in the simulated data. The statistical and background noise were removed for this simulation. The saturation corrections were also removed and constant ozone absorption cross sections were used with values of $\sigma_{O_3 299} = 4.200e^{-23}\,m^2$ and $\sigma_{O_3 289} = 1.542e^{-22}\,m^2$. The correction from Eq. (3) is calculated with the simulated atmospheric number density and constant values of Rayleigh extinction cross sections of $\alpha_{mol299} = 5.730e^{-30}\,m^2$ and $\alpha_{mol289} = 6.661e^{-30}\,m^2$ (Eberhard, 2010). The Rayleigh backscatter volume cross sections in Eq. (2) are then computed from the Rayleigh phase function.

The left panel of Fig. 4, shows the corrected, uncorrected and truth ozone mixing ratio profile. The uncorrected profile indicates a bias of nearly 10 ppbv throughout the entire profile. The right panel of Fig. 4 shows the percent difference for the corrected and uncorrected profiles. Without this correction, the magnitude of this correction is near 20 % in the PBL and 10 % in the free troposphere. This is much more substantial than the temperature dependence of the ozone absorption cross sections, but the correction only varies largely with atmospheric number density and is therefore typically straightforward to correct for. The ozone difference plot in the right panel shows that

AMTD
8, 4273–4305, 2015

this correction is < 1 % if the atmospheric number density is precisely known. For this reason the $TROPOZ_{opt}$ retrieval will implement the updated Rayleigh extinction cross sections.

3.4 Saturation (pulse pile-up)

The TROPOZ retrieval algorithm must also correct for the nonparalyzable dead time correction of the PMTs (Keckhut et al., 2004b). The values used in this simulation are based on the theoretical maximum photon counting rate of the data acquisition system, which is 300 MHz or 3.33 ns. This correction can be applied as,

$$C_t = \frac{C_m}{1 - C_m T_d}, \quad (5)$$

where the true photon count rate (C_t) can be expressed as a function of the measured count rates (C_m) and a dead time (T_d) parameter (Lampton and Bixler, 1985).

When this theoretical value was used with the current retrieval, it did not appear to completely correct for the detector saturation (pulse pile-up). After analyzing this further, a bin registration issue was found in the algorithm which was misrepresenting the quantities of true counts in Eq. (5) throughout the retrieval. This was subsequently adjusted in the final retrieval algorithm before the comparisons were performed with the known ozone profile.

The left panel of Fig. 5 shows the corrected, uncorrected and truth ozone profiles. The right panel shows the percent difference between each of these profiles. The saturation correction is particularly important in the lower regions of each channel and an improper algorithm correction may lead to biases upwards of 20 %. Based on the percent difference plot in the right side of Fig. 5, the difference in this correction is < 1 % and this will be implemented in the $TROPOZ_{opt}$ ozone retrieval. However, the impacts of using a saturation correction may be substantial in the overall retrieval uncertainty and will be discussed in a following paper that will focus on the uncertainty in the TROPOZ measurement.

AMTD
8, 4273–4305, 2015

3.5 TROPOZ$_{opt}$ retrieval algorithm before the addition of statistical noise

After carrying out each of the corrections from the previous sections, it was important to compare the TROPOZ$_{opt}$ retrieval to the known truth profile that was simulated using the combination of each of these corrections. The simulated lidar return signals for this comparison have implemented the effects of the temperature dependence of the ozone absorption cross section, differential Rayleigh extinction between the "on" and "off" channels and saturation (pulse pile-up) of the detectors and the solar background radiation subtraction. The effects of statistical noise have been removed for this simulation. The left panel of Fig. 6 shows the TROPOZ$_{opt}$ retrieval and truth ozone concentration profile. The right panel shows the percent difference between the TROPOZ$_{opt}$ retrieval and known profile without the addition of statistical noise. The spikes in the right panel correspond to abrupt ozone gradients in the simulated ozone profile and are not expected to occur as sharply in the natural atmosphere.

Although it would be physically impossible to determine a percent difference from an atmospheric observation and an ozonesonde, this exercise allows for the TROPOZ$_{opt}$ retrieval biases to be completely quantified before the introduction of real atmospheric noise. The percent differences have been quantified to be mostly within ±1 % of the known ozone profile, which implies that there are no apparent propagating biases in the algorithm between the varying steps of the retrieval described above. However, with the addition of statistical noise, these differences may be much larger and a vertical resolution scheme is presented in the following section to minimize the differences.

4 TROPOZ$_{opt}$ variable vertical resolution scheme and uncertainty analysis

As mentioned before, the TROPOZ retrieval algorithm originally implemented a constant vertical resolution of 375 m below 2.75 km and 750 m above 2.75 km. The left panel of Fig. 7 depicts the new TROPOZ$_{opt}$ retrieval vertical resolution scheme. These values are coupled directly to the FWHM of the steady state SG filter coefficients as-

AMTD
8, 4273–4305, 2015

sociated with the window size as described in the Numerical Derivative section of this paper.

Because a bias naturally occurs due to the decrease in the SNR with altitude, it is favorable to increase the number of points of the derivative low-pass filter used for data processing (Godin et al., 1999). This is evident in the large difference at the join region (near 3 km), in which the lower channel's SNR is decreasing and more data points are needed to provide an accurate ozone profile. However, the adjoining upper channel has a sufficiently high SNR to properly perform the retrieval. The large gradient in the SNR, and therefore the vertical resolution, can mostly be attributed to physical hardware parameters (such as transmitted laser pulse power, telescope diameter, FOV, various optical filters, and the measurement geometry of the TROPOZ system).

The TROPOZ instrument utilizes photon counting data acquisition electronics. The signal collected in this approach follows Poisson statistics (Megie et al., 1985; Papayannis et al., 1990) and the statistical uncertainty of the ozone concentrations is shown in the right panel of Fig. 7. The statistical uncertainty at a given range can be calculated as

$$\epsilon_{N_{O_3}}(r,\lambda) = \frac{1}{2N_{O_3}\Delta\sigma_{O_3}\Delta r_v}\sqrt{\sum_{i=0,1}\ \sum_{j=0,1}\frac{P_{s_i,\lambda_j}+P_{b_i,\lambda_j}+P_{d_i,\lambda_j}}{P^2_{s_i,\lambda_j}}}, \quad (6)$$

where $P_{s,\lambda}$, $P_{b,\lambda}$, and $P_{d,\lambda}$ are the atmospheric backscattered signal, background radiation, and dark counts of the detector at wavelength λ. The vertical resolution, which is based on the smoothing filter window size, is denoted as Δr_v and the differential ozone absorption cross section is denoted as $\Delta\sigma_{O_3}$. The statistical uncertainty is related to the square root of the total PMT counts. The summation is performed for the signal at r and $r + \Delta r_v$, denoted by the index i, and for the "on" and "off" wavelengths, denoted by the index j. By integrating profiles for a longer duration, the SNR of the backscattered signal term $P_{s,\lambda}$ increases and in turn the relative error in ozone number density becomes smaller.

AMTD
8, 4273–4305, 2015

The right panel of Fig. 7 also shows that by increasing the smoothing window used in the retrieved ozone profile, which is in the denominator of Eq. (6), the statistical uncertainty in the measurement can be maintained within a desired limit. Because the vertical resolution changes with altitude and has different values for different channel pairs, the resultant uncertainty profile exhibits the analogous changes. This allows for an optimized vertical resolution scheme to obtain a final statistical uncertainty in the system that is < 10 %. Although a more rigorous and detailed uncertainty analysis will be discussed in the paper in this series, the right panel of Fig. 7 shows an approximation for the overall uncertainty for the $TROPOZ_{opt}$ retrieved ozone concentrations.

5 Comparison of the original TROPOZ and $TROPOZ_{opt}$ retrieval algorithms

The left panel of Fig. 8 shows the original TROPOZ retrieval (Fig. 1), the optimized TROPOZ retrieval ($TROPOZ_{opt}$) and the truth ozone profile. The $TROPOZ_{opt}$ retrieval has implemented all of the changes and corrections described throughout the previous sections of this paper including the optimized vertical resolution scheme from Fig. 7. Improvements in the optimized retrieval are apparent throughout the profile and especially in the region above 4.5 km.

The middle panel of Fig. 8 shows the percent difference between each of the retrievals and the truth profile. Due to the optimized vertical smoothing scheme, the $TROPOZ_{opt}$ algorithm is able to produce ozone profiles nearly 200 m lower (from 675 to 500 m) than the previous TROPOZ retrieval. The bin registration error that was identified with the saturation correction is also adjusted in the final $TROPOZ_{opt}$ retrieval. This adjustment shows a direct reduction in percent difference near the retrieval join regions of nearly 5 % from 675–800 m and 10 % from 2.75 to 3 km. This panel also shows reductions mostly between 5–15 % in the percent difference of the upper tropospheric retrieval as compared to the previous algorithm.

The right panel in Fig. 8 serves as a visual summary to quantify the improvement, or reduction in bias, gained from this optimization process. The improvement was calcu-

AMTD
8, 4273–4305, 2015

lated from the difference in the absolute value of each difference profile in the middle panel Fig. 8, and can be written as,

$$\text{Improvement}_{\%} = |\text{TROPOZ}_{\%}| - |\text{TROPOZ}_{\text{opt}_{\%}}|. \quad (7)$$

The overall profile mean improvement from the original retrieval to the $\text{TROPOZ}_{\text{opt}}$ retrieval (red line) is 3.5 %. In terms of ozone concentrations, this mean improvement is somewhere between 2–4 ppbv. The largest improvements occur in the upper atmosphere where the retrieval performance and vertical resolution were optimized. Specifically, some of the retrieved ozone concentrations above 4.5 km have improved greatly by more than 10 %. Accurate ozone concentrations that are closer to the surface will help add valuable insight to the air quality community and the improved retrieval accuracy above 4.5 km will yield a novel validation source for current and future satellite instruments.

6 Final $\text{TROPOZ}_{\text{opt}}$ retrieval as compared to ozonesondes

After implementing the $\text{TROPOZ}_{\text{opt}}$ retrieval algorithm it was important to analyze real lidar signals that are contaminated with sources of noise. Specifically, this allows for confirmation that the real ambient sky radiation is being correctly accounted for in the final retrieved ozone profile. Although the theoretical dead time correction value is 3.33 ns, based on the counting rate of the transient recorder, this is rarely physically achieved. For this reason, larger values between 4–5 ns are used and were empirically determined by comparing the lidar return signal to a model atmosphere and from ozonesonde measurements.

The first four panels of Fig. 9 show different ozonesonde launches as compared to the new $\text{TROPOZ}_{\text{opt}}$ algorithm and the uncertainty bars represent the statistical uncertainty of the measurement described in Fig. 7. These lidar profiles are ten minute averages and are centered around 19 September 2013 19:03 UTC, 25 October 2013 17:44 UTC, 18 December 2013 17:24 UTC, or 17 April 2014 06:59 UTC, respectively.

AMTD
8, 4273–4305, 2015

The ozonesondes were launched by the Howard University Beltsville Center for Climate Systems Observation. The launch site (39.05° N, 76.88° W) is approximately 8 km from the lidar site which is close enough to assume similar, but not identical tropospheric micrometeorology in the dynamic daytime PBL. These comparison times were chosen to maximize overlap of the two instruments based on the sonde's proximity to the lidar and ascent rate.

In each of the cases, the $TROPOZ_{opt}$ retrieval was able to produce good agreement with the instantaneous ozonesonde profile from 300 m to 10 km. The first $TROPOZ_{opt}$ retrieval, on 19 September 2013 at 19:03 UTC, shows the largest uncertainty than in any of the other four profiles. This is largely because it was retrieved before a hardware modification was made, in which an additional detector was added to better resolve the upper atmosphere. This is an example of how the statistical uncertainty can grow rapidly as the SNR of the system decreases. The following profile, on 25 October 2013 at 17:44 UTC, shows good agreement between the ozonesonde and the $TROPOZ_{opt}$ retrieval, with the largest uncertainty occurring above 9 km. At this altitude, ozone mixing ratio values reaching near 200 ppbv were resolved. This large gradient would not have been resolved as accurately with the original vertical resolution scheme, due to the large decrease in SNR in regions where the return signal was rapidly absorbed by the large concentrations of ozone. On 18 December 2013 at 17:24 UTC, the $TROPOZ_{opt}$ retrieval shows good agreement with the ozonesonde profile for the lower altitude ranges, but begins to differ in the upper altitudes. The final ozonesonde comparison, on 17 April 2014 at 06:59 UTC, shows excellent agreement between the ozonesonde and the $TROPOZ_{opt}$ retrieved ozone mixing ratio. This is a night-time ozonesonde launch, in which the sky background radiation is negligible and the SNR is naturally higher. These combine, with a very low concentration of ozone, to yield a fairly low statistical uncertainty in the measurement.

The fifth panel in Fig. 9 shows the mean percent difference (Diff) for the ECC ozonesonde comparisons presented in the previous four panels. The mean profile was computed from each individual percent difference profile as in Eq. (4), except

AMTD
8, 4273–4305, 2015

the Model$_{N_{O_3}}$ term was replaced with ECC$_{N_{O_3}}$. The blue lines in Fig. 9 represent two standard deviations of the mean relative differences. The TROPOZ$_{opt}$ retrieval is within ±10 % of the ECC ozonesonde throughout most of the retrieved range, which is near the statistical detection limit imposed from the vertical resolution/statistical uncertainty scheme from Fig. 7. The largest differences are near the top of the profile, where the SNR of the measurement is lowest. The gradient near 3 km directly corresponds to the merging of two adjoining altitude channels as describe previously. Finally, because the zero line falls mostly within two standard deviations of the relative differences there is no significant systematic bias present in the TROPOZ$_{opt}$ retrieval algorithm, which is encouraging for future intercomparisons and science investigations.

7 Conclusions

This paper serves as the first paper in a series discussing the optimization of the GSFC TROPOZ DIAL retrieval. This paper is focused on ensuring that the TROPOZ algorithm is accurately quantifying ozone concentrations, as well as develop a primary standard for the retrieval consistency and optimization within TOLNet. The following paper will focus on a robust uncertainty analysis standard for TOLNet instruments. Using simulated lidar returns has shown to be beneficial for testing a new operational version of TROPOZ analysis algorithm. The advantage of using simulated signals is that it is possible to turn varying effects on and off in order to investigate differences between the retrieval and the known truth profile. These differences could never have been truly investigated with actual lidar returns and instantaneous ozonesonde profiles because the state of the atmosphere is never precisely known.

One key improvement from this analysis came from optimizing the vertical resolution scheme from a previously constant resolution. These improvements were upwards of 10 % above 4.5 km. The overall improvement, or reduction in bias, was 3.5 % from the previous retrieval and it was able to extend the lower limit of the range of ozone retrievals by nearly 200 m. Ozone retrievals closer to the surface will help add valu-

AMTD
8, 4273–4305, 2015

able insight to the air quality community and the improved retrieval accuracy above 4.5 km will yield a novel validation source for current and future satellite instruments. The authors believe that this analysis has significantly added to the confidence that the TROPOZ retrieval algorithm is properly quantifying ozone concentrations. Application of this methodology will be recommended to all other TOLNet lidars for validation, optimization, and consistency purposes.

Acknowledgements. The authors wish to gratefully acknowledge the support for this study provided by the NASA Tropospheric Chemistry Program, the Tropospheric Ozone Lidar Network (TOLNET), the Maryland Department of the Environment (Contract U00P7201032), and NOAA-CREST CCNY Foundation CREST Grant (Contract NA11SEC481004.3). Work at the Jet Propulsion Laboratory, California Institute of Technology was done under contract with NASA. Thanks to the Howard University – Beltsville Center for Climate Systems Observation for launching the ozonesondes necessary to continue validating this system. Also, thanks to Raymond M. Hoff for providing extended discussions of lidar techniques.

References

Alvarez, R. J., Senff, C. J., Langford, A. O., Weickmann, A. M., Law, D. C., Machol, J. L., Merritt, D. A., Marchbanks, R. D., Sandberg, S. P., Brewer, W. A., Hardesty, R. M., and Banta, R. M.: Development and application of a compact, tunable, solid-state airborne ozone lidar system for boundary layer profiling, J. Atmos. Ocean. Tech., 28, 1258–1272, 2011. 4276

Ancellet, G., Papayannis, A., Pelon, J., and Megie, G.: DIAL tropospheric ozone measurement using a Nd:YAG laser and the Raman shifting technique, J. Atmos. Ocean. Tech., 6, 832–839, 1989. 4276

Beekmann, M., Ancellet, G., Megie, G., Smit, H., and Kley, D.: Intercomparison campaign of vertical ozone profiles including electrochemical sondes of ECC and Brewer-Mast type and a ground based UV-differential absorption lidar, J. Atmos. Chem., 19, 259–288, doi:10.1007/BF00694614, 1994. 4277

Browell, E. V., Ismail, S., and Shipley, S. T.: Ultraviolet DIAL measurements of O_3 profiles in regions of spatially inhomogeneous aerosols, Appl. Optics, 24, 2827–2836, available at: http://ao.osa.org/abstract.cfm?URI=ao-24-17-2827, 1985. 4279

AMTD
8, 4273–4305, 2015

Boor, C. D.: A Practical Guide to Splines, Mathematics of Computation, 1978. 4283
Eberhard, W. L.: Correct equations and common approximations for calculating Rayleigh scatter in pure gases and mixtures and evaluation of differences, Appl. Optics, 49, 1116–1130, 2010. 4284
Godin, S., Carswell, A. I., Donovan, D. P., Claude, H., Steinbrecht, W., McDermid, I. S., McGee, T. J., Gross, M. R., Nakane, H., Swart, D. P. J., Bergwerff, H. B., Uchino, O., von der Gathen, P., and Neuber, R.: Ozone differential absorption lidar algorithm intercomparison, Appl. Optics, 38, 6225–6236, available at: http://ao.osa.org/abstract.cfm?URI=ao-38-30-6225, 1999. 4287
Hedin, A. E.: Extension of the MSIS thermosphere model into the middle and lower atmosphere, J. Geophys. Res.-Space, 96, 1159–1172, 1991. 4280
IPCC: Climate Change 2007 – The Physical Science Basis: Working Group I Contribution to the Fourth Assessment Report of the IPCC, Climate Change 2007, Cambridge University Press, 2007. 4275
Keckhut, P., McDermid, S., Swart, D., McGee, T., Godin-Beekmann, S., Adriani, A., Barnes, J., Baray, J.-L., Bencherif, H., Claude, H., di Sarra, A. G., Fiocco, G., Hansen, G., Hauchecorne, A., Leblanc, T., Lee, C. H., Pal, S., Megie, G., Nakane, H., Neuber, R., Steinbrecht, W., and Thayer, J.: Review of ozone and temperature lidar validations performed within the framework of the Network for the Detection of Stratospheric Change, J. Environ. Monit., 6, 721–733, doi:10.1039/B404256E, 2004a. 4277
Keckhut, P., McDermid, S., Swart, D., McGee, T., Godin-Beekmann, S., Adriani, A., Barnes, J., Baray, J.-L., Bencherif, H., Claude, H., di Sarra, A. G., Fiocco, G., Hansen, G., Hauchecorne, A., Leblanc, T., Lee, C. H., Pal, S., Megie, G., Nakane, H., Neuber, R., Steinbrecht, W., and Thayer, J.: Review of ozone and temperature lidar validations performed within the framework of the Network for the Detection of Stratospheric Change, J. Environ. Monit., 6, 721–733, doi:10.1039/B404256E, 2004b. 4285
Komhyr, W. D., Barnes, R. A., Brothers, G. B., Lathrop, J. A., and Opperman, D. P.: Electrochemical concentration cell (ECC) ozonesonde pump efficiency measurements and tests on the sensitivity to ozone of buffered and unbuffered ECC sensor cathode solutions, J. Geophys. Res.-Atmos., 100, 9231–9244, doi:10.1029/94JD02175, 1995. 4276
Kuang, S., Newchurch, M. J., Burris, J., and Liu, X.: Ground-based lidar for atmospheric boundary layer ozone measurements, Appl. Optics, 52, 3557–3566, 2013. 4276

AMTD
8, 4273–4305, 2015

Lampton, M. and Bixler, J.: Counting efficiency of systems having both paralyzable and non-paralyzable elements, Rev. Sci. Instrum., 56, 164–165, 1985. 4285
Langford, A. O., Senff, C. J., Alvarez, R. J., Banta, R. M., and Hardesty, R. M.: Long-range transport of ozone from the Los Angeles Basin: a case study, Geophys. Res. Lett., 37, L0687, doi:10.1029/2010GL042507, 2010. 4275
Leblanc, T., McDermid, I. S., Hauchecorne, A., and Keckhut, P.: Evaluation of optimization of lidar temperature analysis algorithms using simulated data, J. Geophys. Res.-Atmos., 103, 6177–6187, doi:10.1029/97JD03494, 1998. 4277
Malicet, J., Daumont, D., Charbonnier, J., Parisse, C., Chakir, A., and Brion, J.: Ozone UV spectroscopy. I I. Absorption cross-sections and temperature dependence, J. Atmos. Chem., 21, 263–273, doi:10.1007/BF00696758, 1995. 4282, 4283
McDermid, I. S., Beyerle, G., Haner, D. A., and Leblanc, T.: Redesign and improved performance of the tropospheric ozone lidar at the Jet Propulsion Laboratory Table Mountain Facility, Appl. Optics, 41, 7550–7555, 2002. 4276
McDonnell, W. F., Abbey, D. E., Nishino, N., and Lebowitz, M. D.: Long-term ambient ozone concentration and the incidence of asthma in nonsmoking adults: The AHSMOG study, Environ. Res., 80, 110–121, 1999. 4275
Megie, G. J., Ancellet, G., and Pelon, J.: Lidar measurements of ozone vertical profiles, Appl. Optics, 24, 3454–3463, 1985. 4278, 4287
Newchurch, M. J., Ayoub, M. A., Oltmans, S., Johnson, B., and Schmidlin, F. J.: Vertical distribution of ozone at four sites in the United States, J. Geophys. Res.-Atmos., 108, ACH 9-1–9-17, doi:10.1029/2002JD002059, 2003. 4276
Papayannis, A., Ancellet, G., Pelon, J., and Mégie, G.: Multiwavelength lidar for ozone measurements in the troposphere and the lower stratosphere, Appl. Optics, 29, 467–476, 1990. 4287
Pliutau, D. and De Young, R.: UV lidar receiver analysis for tropospheric sensing of ozone, Technical Manual 218038, NASA, 2013. 4276
Savitzky, A. and Golay, M. J. E.: Smoothing and differentiation of data by simplified least squares procedures, Anal. Chem., 36, 1627–1639, available at: doi:10.1021/ac60214a047, 1964. 4282
Smit, H. G. J., Straeter, W., Johnson, B. J., Oltmans, S. J., Davies, J., Tarasick, D. W., Hoegger, B., Stubi, R., Schmidlin, F. J., Northam, T., Thompson, A. M., Witte, J. C., Boyd, I., and Posny, F.: Assessment of the performance of ECC-ozonesondes under

AMTD
8, 4273–4305, 2015

quasi-flight conditions in the environmental simulation chamber: insights from the Juelich Ozone Sonde Intercomparison Experiment (JOSIE), J. Geophys. Res.-Atmos., 112, D19306, doi:10.1029/2006JD007308, 2007. 4276

Stevenson, D. S., Young, P. J., Naik, V., Lamarque, J.-F., Shindell, D. T., Voulgarakis, A., Skeie, R. B., Dalsoren, S. B., Myhre, G., Berntsen, T. K., Folberth, G. A., Rumbold, S. T., Collins, W. J., MacKenzie, I. A., Doherty, R. M., Zeng, G., van Noije, T. P. C., Strunk, A., Bergmann, D., Cameron-Smith, P., Plummer, D. A., Strode, S. A., Horowitz, L., Lee, Y. H., Szopa, S., Sudo, K., Nagashima, T., Josse, B., Cionni, I., Righi, M., Eyring, V., Conley, A., Bowman, K. W., Wild, O., and Archibald, A.: Tropospheric ozone changes, radiative forcing and attribution to emissions in the Atmospheric Chemistry and Climate Model Intercomparison Project (ACCMIP), Atmos. Chem. Phys., 13, 3063–3085, doi:10.5194/acp-13-3063-2013, 2013. 4275

Sullivan, J. T., McGee, T. J., Sumnicht, G. K., Twigg, L. W., and Hoff, R. M.: A mobile differential absorption lidar to measure sub-hourly fluctuation of tropospheric ozone profiles in the Baltimore–Washington, D.C. region, Atmos. Meas. Tech., 7, 3529–3548, doi:10.5194/amt-7-3529-2014, 2014. 4276

Sullivan, J. T., McGee, T. J., De Young, R., Sumnicht, G. K., Twigg, L. W., Pliutau, D., Carrion, W., and Knepp, T.: Results from the NASA GSFC and LaRC ozone lidar intercomparison: new mobile tools for atmospheric research, J. Atmos. Ocean. Tech., submitted, 2015. 4276

The National Climate Assessment and Development Advisory Committee (NCADAC) Draft Climate Assessment Report, available at: http://ncadac.globalchange.gov/, 2013. 4275

Thompson, A. M., Witte, J. C., McPeters, R. D., Oltmans, S. J., Schmidlin, F. J., Logan, J. A., Fujiwara, M., Kirchhoff, V. W. J. H., Posny, F., Coetzee, G. J. R., Hoegger, B., Kawakami, S., Ogawa, T., Johnson, B. J., Vömel, H., and Labow, G.: Southern Hemisphere Additional Ozonesondes (SHADOZ) 1998–2000 tropical ozone climatology 1. Comparison with Total Ozone Mapping Spectrometer (TOMS) and ground-based measurements, J. Geophys. Res.-Atmos., 108, PEM 10-1–PEM 10-19, doi:10.1029/2001JD000967, 2003. 4276

Thuburn, J.: UGAMP Internal Report, Tech. Rep. 16, University of Exeter, Exeter, UK, 1992. 4281

Uchino, O., Sakai, T., Nagai, T., Morino, I., Maki, T., Deushi, M., Shibata, K., Kajino, M., Kawasaki, T., Akaho, T., Takubo, S., Okumura, H., Arai, K., Nakazato, M., Matsunaga, T., Yokota, T., Kawakami, S., Kita, K., and Sasano, Y.: DIAL measurement of lower tropospheric

AMTD
8, 4273–4305, 2015

ozone over Saga (33.24° N, 130.29° E), Japan, and comparison with a chemistry–climate model, Atmos. Meas. Tech., 7, 1385–1394, doi:10.5194/amt-7-1385-2014, 2014. 4276

US Standard: US Standard Atmosphere, 1976. Adopted by the United States Committee on Extension to the Standard Atmosphere, National Oceanic and Amospheric Administration. U. S. Govt. Print. Off., Washington, 1976. 4279

AMTD

8, 4273–4305, 2015

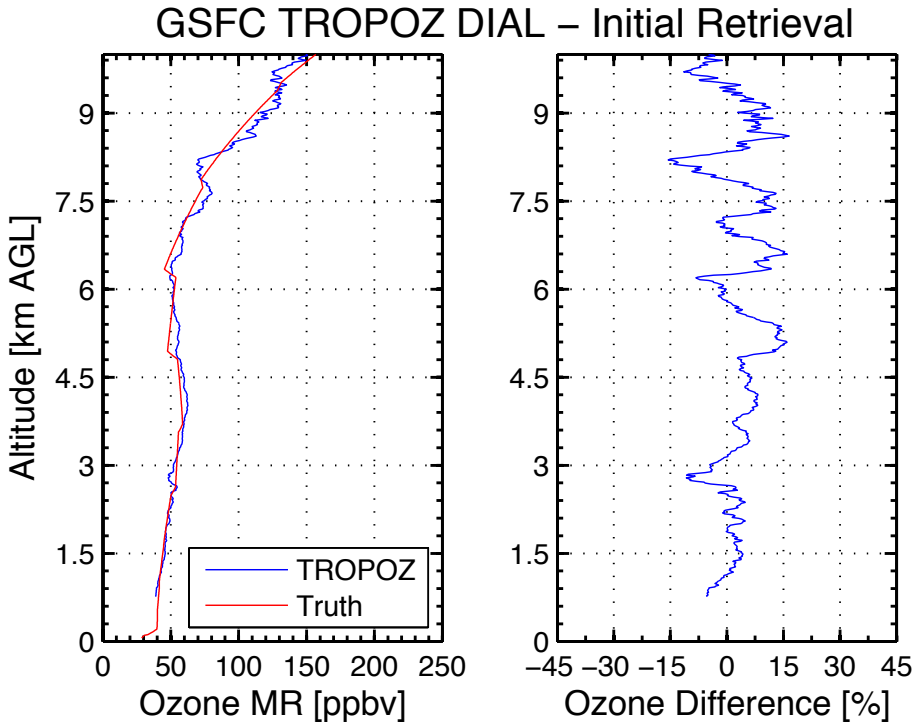

Figure 1. The left panel shows the initial retrieved ozone concentration from the TROPOZ algorithm as compared to the known ozone profile used in the simulated lidar return signals. The right panel shows the percent difference from the known profile and retrieved profile.

AMTD
8, 4273–4305, 2015

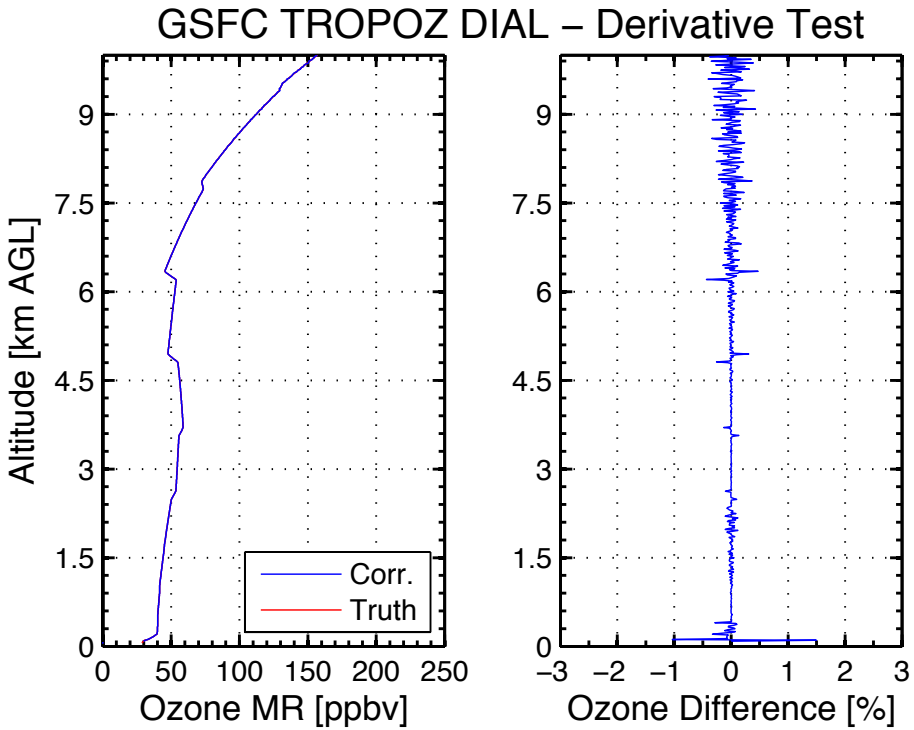

Figure 2. The left panel shows the initial retrieved ozone concentration from the TROPOZ algorithm using the Savitzky–Golay differentiation filter for the numerical derivative as compared to the known ozone profile used in the simulated lidar return signals. The right panel shows the percent difference from the known profile and retrieved profile.

AMTD
8, 4273–4305, 2015

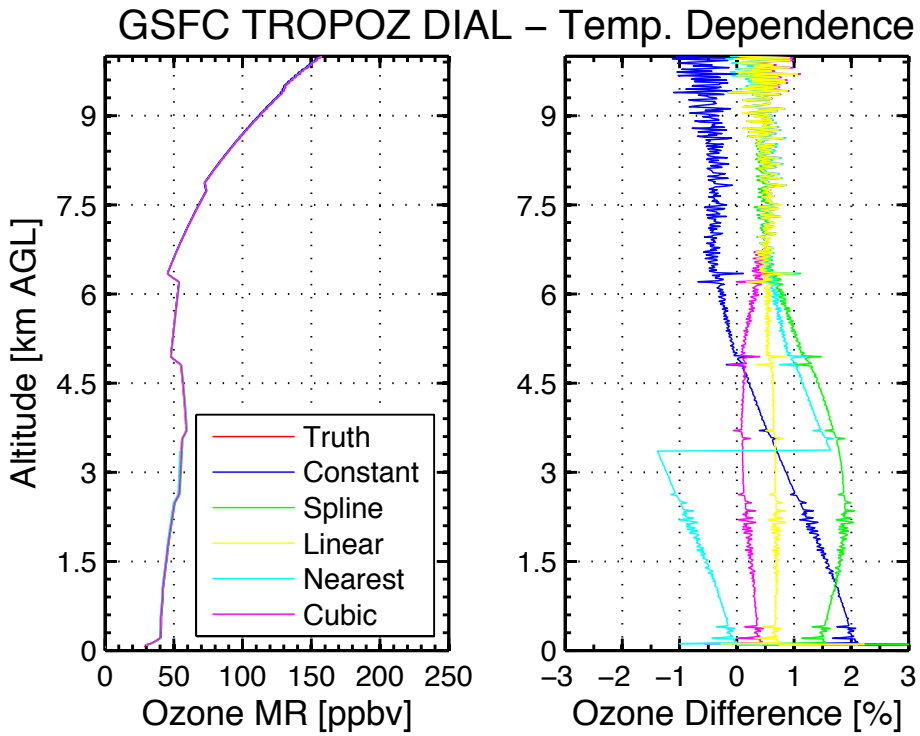

Figure 3. The left panel shows the retrieved ozone mixing ratio from the varying TROPOZ interpolations of the temperature dependence of ozone absorption cross sections as compared to the known ozone profile used in the simulated lidar return signal. The right panel shows the percent difference from the known profile and the retrieved profile using various temperature interpolations.

AMTD
8, 4273–4305, 2015

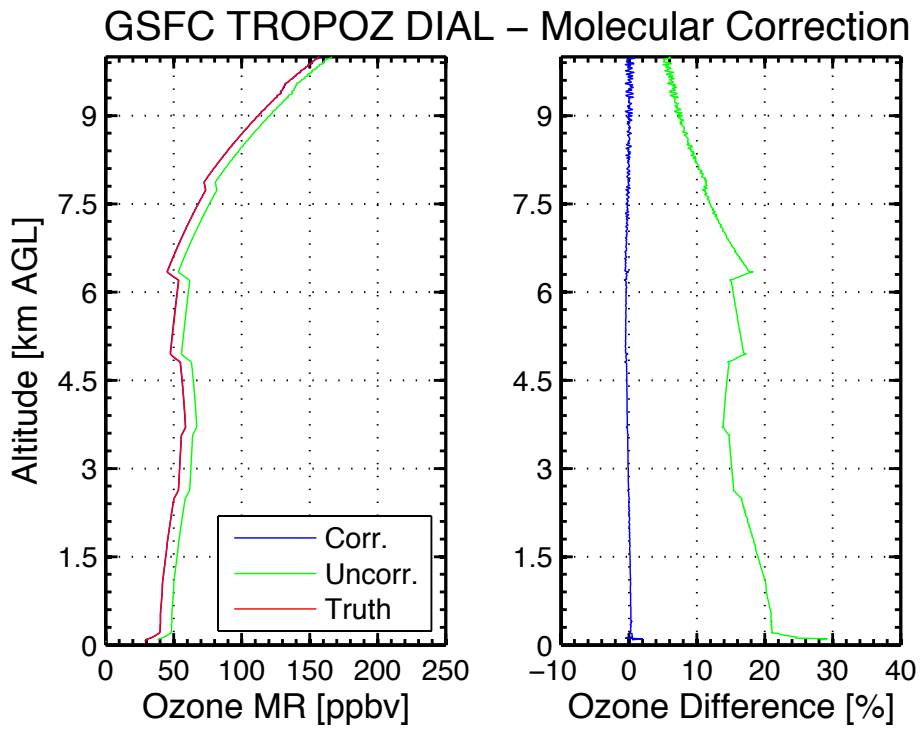

Figure 4. The left panel shows the retrieved ozone mixing ratios from the corrected and uncorrected TROPOZ ozone profiles as compared to the known ozone profile used in the simulated lidar return signal. The right panel shows the percent difference from the known profile and retrieved profiles.

AMTD
8, 4273–4305, 2015

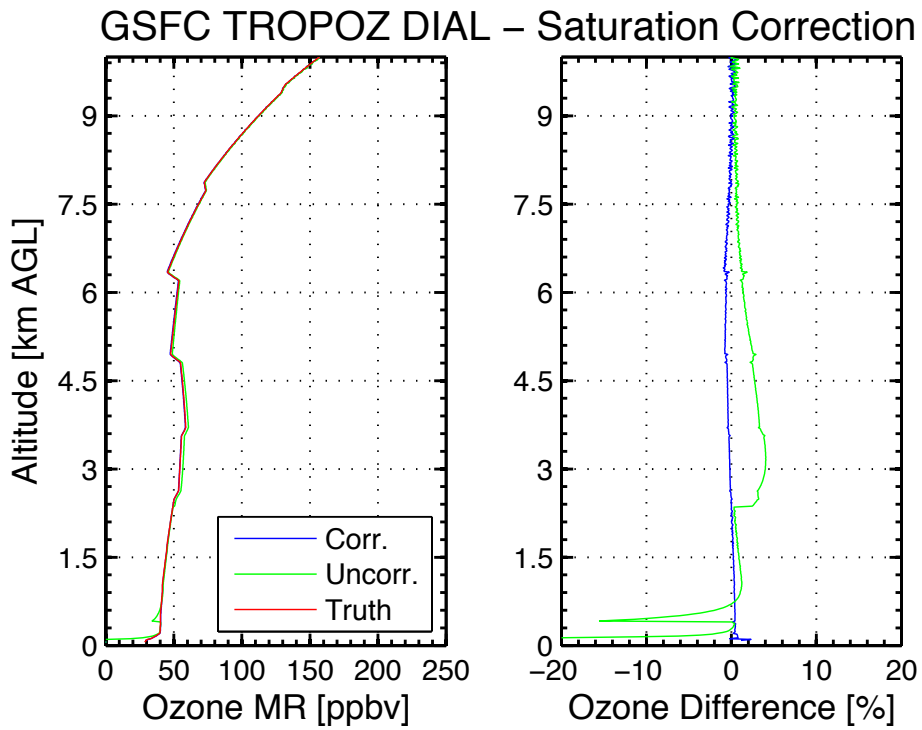

Figure 5. The left panel shows the retrieved ozone mixing ratios from the saturation corrected and uncorrected TROPOZ ozone profiles as compared to the known ozone profile used in the simulated lidar return signal. The right panel shows the percent difference from the known profile and retrieved profiles.

AMTD
8, 4273–4305, 2015

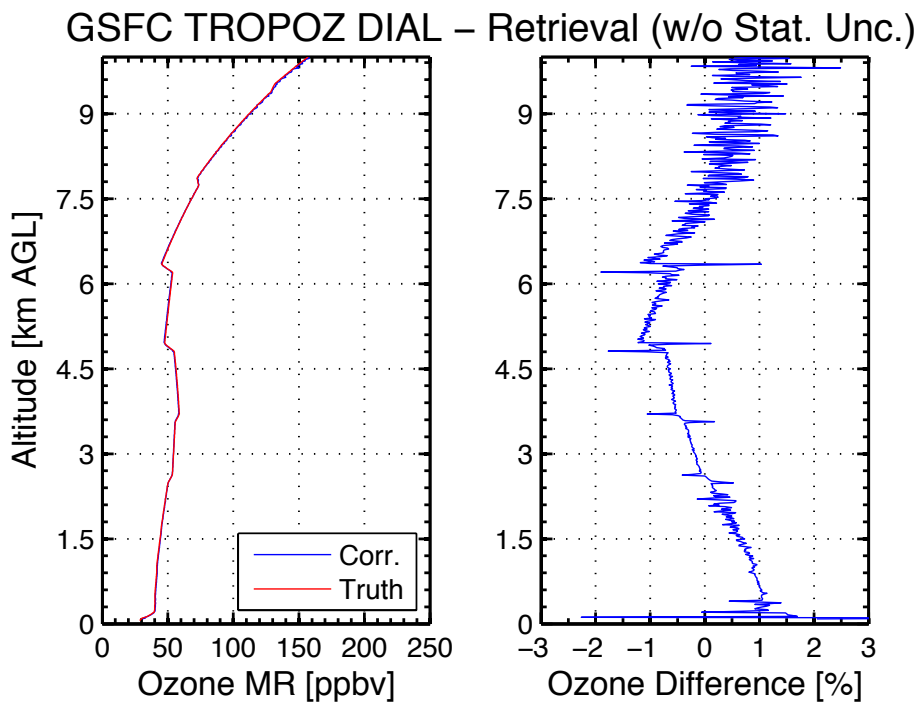

Figure 6. The left panel shows the retrieved ozone mixing ratios from the corrected $TROPOZ_{opt}$ retrieved ozone profiles as compared to the known ozone profile used in the simulated lidar return signal without the addition of statistical noise. The right panel shows the percent difference from the known profile and retrieved profile.

AMTD
8, 4273–4305, 2015

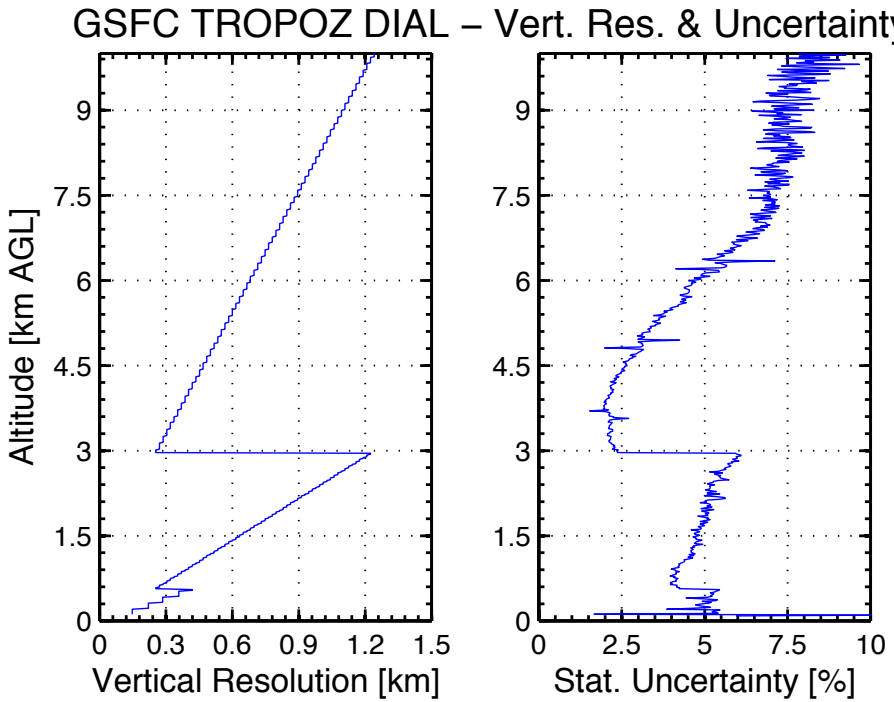

Figure 7. The left panel shows the associated vertical resolution in the $TROPOZ_{opt}$ retrieval algorithm which is derived from the windows size of the SG differentiation filter. The right panel shows the statistical uncertainty in the system associated with these vertical resolutions, which is an approximation for the overall uncertainty for the $TROPOZ_{opt}$.

AMTD
8, 4273–4305, 2015

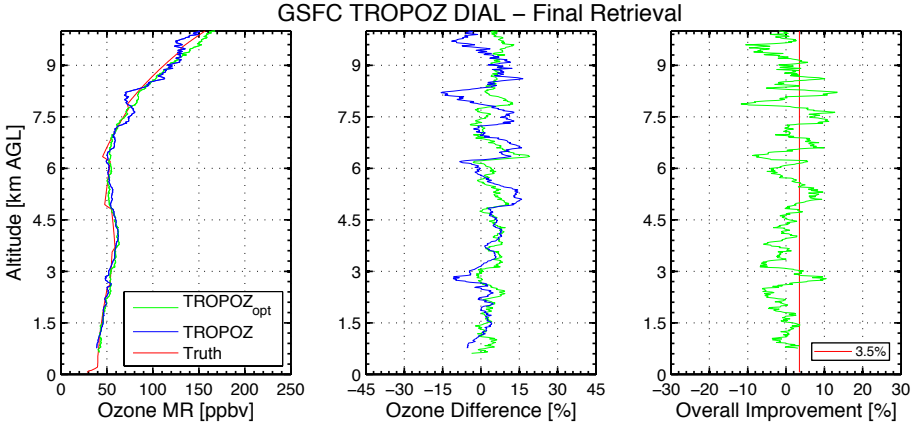

Figure 8. The left panel compares the final retrieved ozone concentration from the previous TROPOZ retrieval and the optimized retrieval ($TROPOZ_{opt}$) to the known ozone profile used in the simulated lidar return signal. The center panel shows the differences in percentage from the known profile and retrieved TROPOZ and $TROPOZ_{opt}$ profiles. The right panel shows the improvement from the optimized $TROPOZ_{opt}$ retrieval from the original TROPOZ retrieval in percentage. The mean improvement (red line), or reduction in overall bias, is 3.5 %.

AMTD
8, 4273–4305, 2015

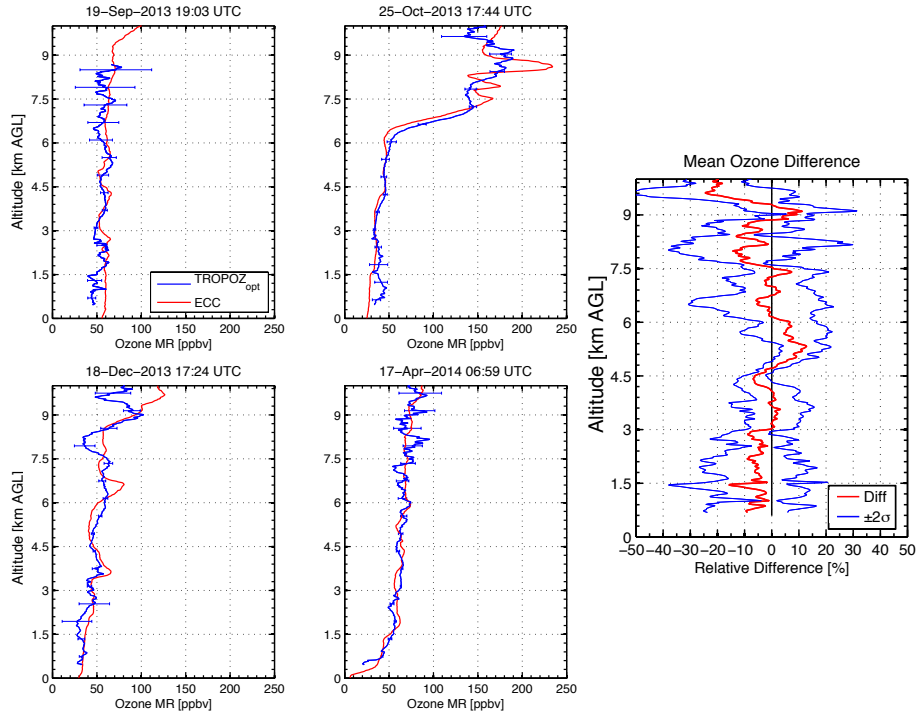

Figure 9. Comparisons between four nearby ECC ozonesonde launches and the updated TROPOZ$_{opt}$ retrieval algorithm (four left panels) and the mean relative percentage difference for all of the comparisons (right panel).

AMTD
8, 4273–4305, 2015